11th International Conference
1-3 July 2013
Pisa
RASD 2013

NONLINEAR VIBRATIONS OF A STROKE-SATURATED INERTIAL ACTUATOR

L. I. Wilmshurst[1*], M. Ghandchi-Tehrani[1] and S. J. Elliott[1]

[1]Institute of Sound and Vibration Research
University of Southampton
Southampton, UK
E-mail: lw5e10@soton.ac.uk

Keywords: Nonlinear dynamics, actuators, stroke saturation.

ABSTRACT

Proof-mass actuators are typically used to supply an external control force to a structure, for the purpose of vibration suppression. These devices comprise a proof-mass suspended in a magnetic field that is accelerated in order to provide a reaction force on the actuator casing and the structure itself. If the actuator stroke length is reached or exceeded, the proof-mass will hit the end stops, resulting in a nonlinear phenomenon known as stroke saturation. In this paper, a theoretical and experimental investigation into the actuator's dynamical behaviour is undertaken. First, the blocked inertial force of the actuator in response to an input voltage was measured experimentally using a variety of excitation amplitudes and frequencies. An analysis was conducted in the time- and frequency-domains, and the first-order force-voltage FRF of the actuator was ascertained for each excitation amplitude. The information provided by the analysis was then used to estimate the parameters for a linear piecewise stiffness model of the actuator, in order to simulate the time-domain response. Finally, a comparison of the simulated and measured signals is conducted to establish the accuracy of the model.

1. INTRODUCTION

The extensive use of light, flexible structures in recent times has necessitated the use of active vibration control, since passive control methods typically add mass to the structure, thereby conflicting with the requirements for lightness and flexibility. Instead, the velocity or displacement of the structure is fed back to a collocated actuator for the purpose of increasing the effective stiffness or damping of the structure [1]. Proof-mass actuators, which generate a control force by means of accelerating a proof-mass in response to an input voltage, are highly advantageous for this purpose due to the relatively large force-to-weight ratio [2]. However, the displacement of the proof-mass is limited by the actuator stroke length; if the input voltage is large, the proof-mass will collide with the end stops, thereby saturating the displacement amplitude [3].

There are a number of reasons why this phenomenon, known as stroke saturation, is undesirable. Firstly, when stroke saturation occurs, large shocks are transmitted to the structure and damage to the actuator may occur. Secondly, it limits the effective control force that can be applied by the actuator to the structure. Thirdly, it has been shown in practice that stoke saturation can lead to destabilisation in the closed-loop system [4]. This is particularly problematic for systems that are subjected to potentially large disturbances, such as seismic

waves, and so it is desirable that the actuators remain stable for large inputs [5].

Recently, Baumann and Elliott [4] modelled a proof-mass actuator using a lumped parameter system with a nonlinear spring, where the spring stiffness becomes very large during stroke saturation. Using this model, it was demonstrated that when the actuator is used to apply velocity feedback control to a structure, the closed-loop system is unstable for large impulsive inputs. However, there were a number of drawbacks with the model. Firstly, it was assumed that the actuator behaves as a linear single-degree-of-freedom system for low input amplitudes, where stroke saturation does not occur. Secondly, it was uncertain whether the function used to model the spring stiffness accurately represented stroke saturation.

In this study, the dynamics of the proof-mass actuator itself are examined in greater detail, for the purpose of developing a model of the stroke-saturated inertial actuator based on measurements. It is shown using experimental measurements that the actuator behaves as a weakly nonlinear system beneath the saturation threshold, and that a linear piecewise model can be used to simulate the general actuator response. The model parameters are obtained from the measurements using curve-fitting techniques and impact modelling procedures, and so the experimental results are shown earlier in the paper than the simulated results. Section 2 outlines the motivations and objectives. Section 3 covers the experimental measurements and procedures used in the study. The modelling process is discussed in section 4, and comparisons between the model simulations and the measurements are made in section 5. Section 6 gives conclusions and future work.

2. MOTIVATION AND OBJECTIVES

As stated in the previous section, the primary objectives of this work are to characterise the nonlinear dynamics of the actuator using time- and frequency-domain analysis, and to develop a model of the actuator that accounts for these dynamics. It is important to include the nonlinear actuator dynamics when applying active vibration control to a structure, since they will affect the response and stability of the closed-loop system. By developing an actuator model that can accurately represent the effects of stroke saturation, the next step would be to design a nonlinear controller that enables the closed-loop system to remain stable, regardless of the stroke saturation effects.

The actuator dynamics are defined by the force-time signal f imparted by the actuator to a structure when the actuator is subjected to a time-varying voltage signal v_{in}. By assuming that the dynamics of the supporting structure is sufficiently rigid at low frequencies, the force is blocked, and the dynamics of the supporting structure can be ignored.

Since the effects of nonlinearities are more obvious with the use of sinusoidal excitation [6], stepped sine excitation of the form $v_{in} = \mathrm{V}_{in} \sin(\omega t)$ was used. Experiments have confirmed that severe harmonic distortion occurs in the force-time signals as V_{in} increases, thereby indicating the presence of stroke saturation. Furthermore, a less pronounced form of harmonic distortion occurs for lower excitation amplitudes, which suggests that the actuator behaves as a weakly nonlinear system beneath the saturation threshold. In both cases, harmonic distortion is most noticeable when the excitation frequency ω is close to the peak resonance frequency of the proof-mass suspension system, denoted by $\omega_{\max}$.

It is important that the actuator model accounts for both of these types of nonlinearities, yet the focus of this paper remains solely on the saturation nonlinearity. In previous work, stroke saturation is typically modelled as a hard clipping effect [2, 3] as a means of assessing the closed-loop performance and stability. However, it is believed that stroke saturation can be modelled more effectively by viewing the impact of the proof-mass and the end stop as an elastic collision between two rigid bodies. Recently, Nagurka and Huang [7] presented a bouncing ball model that relates various impact parameters, such as the contact time and the coefficient of restitution, to additional stiffness and damping terms. By applying these methods in this study, it is evident that stroke saturation can be viewed as a change in stiffness

and damping. The result is a linear piecewise model that is similar in principle to the model derived by Baumann and Elliott [4]. An illustration of the model is shown in Figure 1(b).

(a) 

(b) 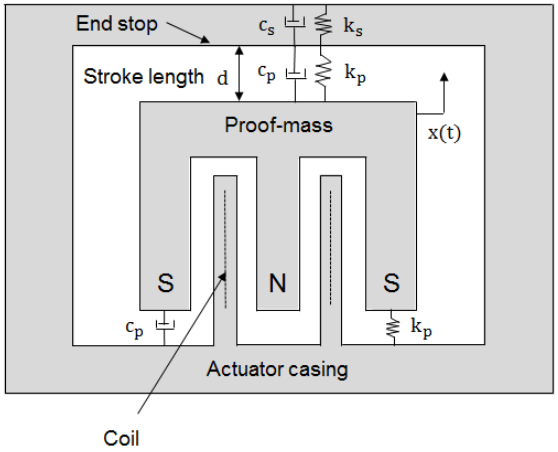

Figure 1. Illustration of (a) the experimental setup and (b) the equivalent model. The suspension stiffness and damping are represented by the parameters k_p and c_p respectively, and the impact parameters are represented by k_s and c_s.

Comparisons between simulations generated from the model and the measurements are initially conducted in the time-domain, in order to examine the signals for harmonic distortion. Further comparisons are made in the frequency-domain, where the spectra of the force-time signals are analysed for information on the harmonics, including spacing, relative strength, and envelope shape. Finally, the simulated and measured signals are used to obtain the first-order force-voltage FRFs of the actuator [8], which convey the force-voltage amplitude ratio at the fundamental excitation frequency ω by ignoring the additional higher-order harmonics in the force signal. These FRFs are taken for the purpose of establishing how the peak resonance frequency of the actuator varies with excitation amplitude.

3. EXPERIMENTS

The experiments were carried out on a Micromega Dynamics IA-01 inertial actuator, which was attached horizontally to an approximately rigid steel block via a Dytran 1053V2 force sensor, as shown in Figure 1(a), in order to measure the blocked force of the actuator. Source generation and data acquisition tasks were performed in MATLAB through the use of a National Instruments NI-cRIO-9623 I/O module. The input voltage signal was amplified by a Micromega Dynamics Rack-04-45N prior to driving the inertial actuator, and the force sensor output signal was conditioned by a Dytran 4102C signal conditioner.

The time histories of the conditioned force sensor signal and the input voltage signal were recorded over a period of ten seconds, using a sampling rate of 51.2 kHz, to obtain the measured signals. These signals were obtained over a range of input frequencies from 5 Hz to approximately 50 Hz using stepped-sine excitation, whilst maintaining a constant excitation amplitude. The excitation frequency vector $\omega(n)$ used had a variable resolution, given by:

$$\omega(n) = 10\pi \cdot 1.02^{n-1} \tag{1}$$

where n is the index number. Using Eq. (1), the highest resolution (0.1 Hz) was achieved at the lowest frequencies, near the peak resonance, whereas the lowest resolution (1 Hz)

occurred at the highest frequencies that were well away from the peak resonance. Initially, a low excitation amplitude $V_{in} = 0.1\,\text{V}$ was used to drive the actuator, in order to obtain an approximately monoharmonic response. The excitation amplitude was then increased in increments of $0.1\,\text{V}$, such that harmonic distortion was more pronounced in the measurements as a result of stroke saturation and other weak nonlinearities. The largest excitation amplitude used was $V_{in} = 0.6\,\text{V}$, which was just beneath the saturation threshold of the amplifier.

In order to obtain f and v_{in} from the measured signals, it is necessary to consider the equipment dynamics, which is assumed to be linear and time-invariant. The FRFs of the equipment were measured using stepped-sine excitation over 5 - 50 Hz. To avoid issues with the counter-electromotive force generated by the actuator, a 3Ω resistor was used to approximate the impedance of the actuator [9] for the amplifier FRF measurement, assuming that the reactance is negligible in this frequency region.

The measurements indicated that the gain and phase changes imparted by the signal conditioner and the I/O module are small enough to be negated. In addition, the amplifier gain (11 dB) and force sensor sensitivity (22.48 mV/N) were approximately independent of frequency across the range of interest. Thus, f can be obtained from the measured output signal by taking the force sensor sensitivity into account, and v_{in} is obtained directly from the measured input signal.

In the frequency domain, the first-order force-voltage FRFs were obtained from the spectra of the force and voltage signals by noting the complex amplitudes of f and v_{in} at the corresponding excitation frequency ω, and repeating the process for all excitation frequencies, where f and v_{in} are changed accordingly. Since the FRFs are characterised for a single excitation amplitude, it is imperative that V_{in} remains constant as ω changes. It should also be noted that the input signal is taken before the amplifier in order to avoid the aforementioned counter-electromotive force generated by the actuator, and so the amplifier dynamics are included in the FRF measurements. If necessary, the amplifier dynamics can be removed from the FRF by taking the reciprocal of the amplifier gain.

3.1 Time-Domain Results

In order to examine the effects of harmonic distortion on the force-time signals, a time-domain analysis is conducted. Figure 2 illustrates the force-time histories of the actuator when subjected to various monoharmonic excitation signals. Two excitation frequencies were considered, one of which was very close to the peak resonance frequency $\omega_{\max}$ ($\omega = 16\pi$ rad/s) [9], and the other was well away from $\omega_{\max}$ ($\omega = 26\pi$ rad/s). Since stroke saturation does not occur for low excitation amplitudes, the initial excitation amplitude used was $V_{\text{in}} = 0.3\,\text{V}$, such that the effects of weak nonlinearities could be distinguished from stroke saturation. The higher excitation amplitudes $V_{\text{in}} = 0.4, 0.5\,\text{V}$ were also considered so that the effects of stroke saturation could be observed.

In Figure 2, harmonic distortion is most noticeable for $\omega = 16\pi$ rad/s. It is apparent that at higher excitation amplitudes, spikes start to appear in the force-time histories, where the acceleration changes rapidly as a result of the proof-mass colliding with the end stop. Therefore, the appearance of spikes in the force-time signals indicates the presence of stroke saturation. The magnitude of these spikes appears to increase with excitation amplitude. Furthermore, the spikes are asymmetrical in the x-axis, which implies that the proof-mass collides with one particular end stop rather than both of them.

For $\omega = 16\pi$ rad/s, it is evident that harmonic distortion is present in the force-time signal even at the lower excitation amplitude $V_{\text{in}} = 0.3\,\text{V}$. Judging by the lack of spikes in the signal, the excitation amplitude is not high enough for stroke saturation to occur, and therefore, it is

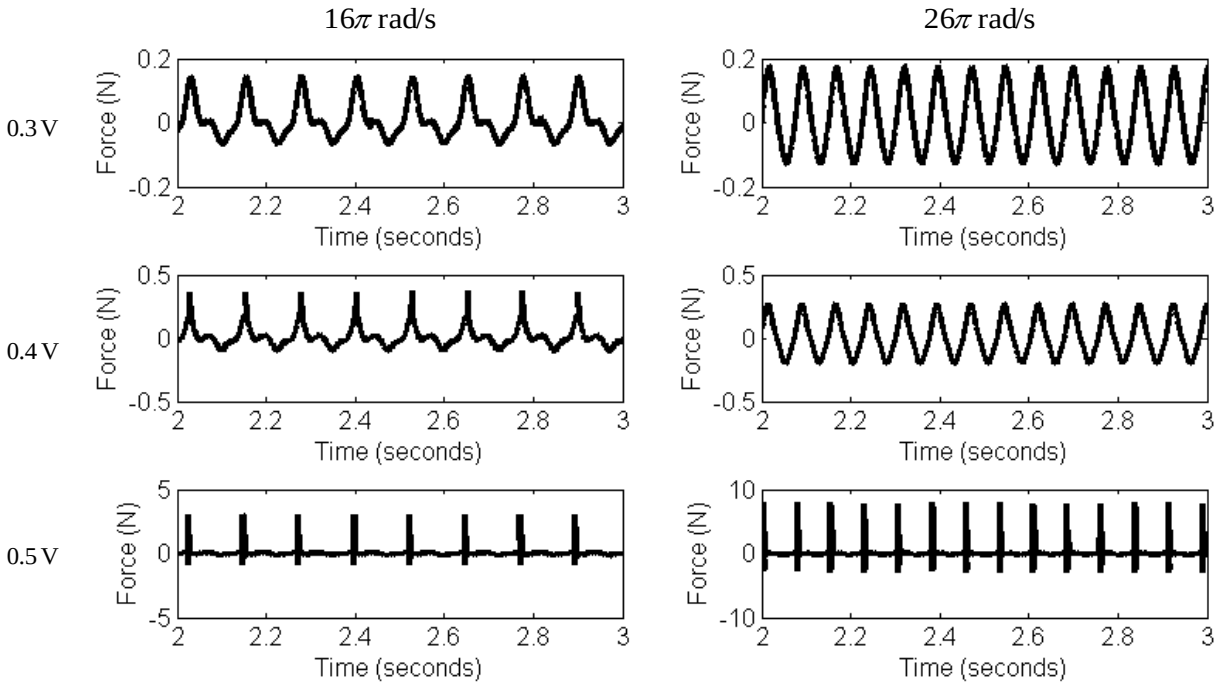

Figure 2. Measured force-time histories of the actuator at various drive voltages for two input frequencies.

suggested that the harmonic distortion is caused by weak nonlinearities in the actuator suspension. This observation is confirmed in the frequency-domain later.

For $\omega = 26\pi$ rad/s, harmonic distortion is far less obvious in the time-domain signals, as ω is further away from $\omega_{\max}$. In addition, spikes do not appear until $V_{in} = 0.5$ V is reached, thereby indicating that the saturation threshold is frequency-dependent. When the excitation frequency is well away from the peak resonance, higher excitation amplitudes can be used before stroke saturation occurs.

3.2 Frequency-Domain Results

It was suggested in the previous section that there are two nonlinear processes that introduce harmonic distortion in the actuator force-time signals; stoke saturation, which severely distorts the signals, and suspension nonlinearities, which have a weaker, but still noticeable effect. Both of these nonlinearities introduce additional harmonics into the force-time signals, and by analysing the spectra of these signals, the nature of the nonlinearities can be revealed in greater detail. In order to consider the nonlinearities separately, the spectra of two force-time signals in Figure 2 are examined. The first signal ($\omega = 16\pi$ rad/s, $V_{in} = 0.3$ V) indicates the presence of suspension nonlinearities without stroke saturation, whereas the second signal ($\omega = 26\pi$ rad/s, $V_{in} = 0.5$ V) is primarily subject to stroke saturation, with negligible distortion from the suspension nonlinearities. The spectra are shown in Figures 3(a) and 3(b) respectively.

It is apparent in Figure 3(a) that the weak nonlinearity manifests itself as several harmonics that decrease in magnitude until the noise floor is reached, thereby indicating that the nonlinearity can be modelled using low-order polynomial terms [6]. The continuous train of harmonics in Figure 3(b) are almost entirely a result of the stroke saturation spikes in the time histories; the rectangular spike shape controls the envelope of the harmonics in a manner akin to a sinc function, and the periodicity of the spikes generates the harmonics themselves. This indicates that stroke saturation is a strongly nonlinear process, as is expected.

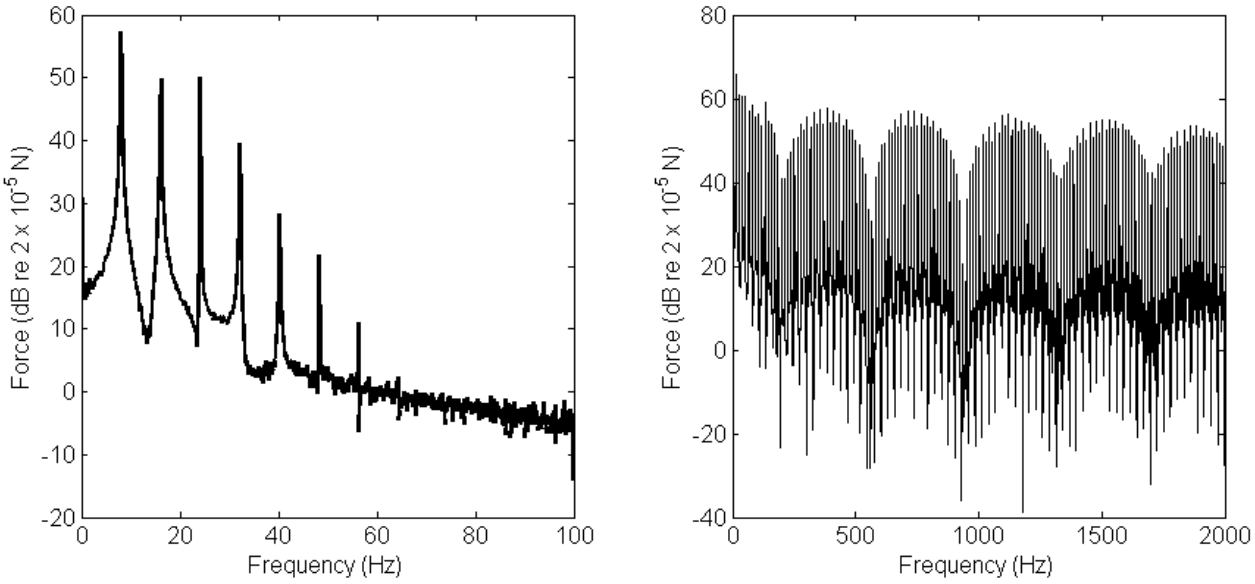

Figure 3. Spectral content of two of the force-time histories shown in Figure 2, for (a) ($\omega = 16\pi$ rad/s, $V_{in} = 0.3$ V) and (b) ($\omega = 26\pi$ rad/s, $V_{in} = 0.5$ V). In both cases, the Fourier transform of the time-domain signal was taken after a Hanning window was applied.

Although Figure 3(a) confirms that the actuator is weakly nonlinear beneath the saturation threshold, there is little indication of the physical processes within the actuator that result in the nonlinearity. One possible explanation is to assume that the stiffness of the suspension spring varies with the proof-mass displacement, which would appear in the first-order force-voltage FRFs as changes in the peak resonance frequency with increasing excitation amplitude [6]. The magnitude and phase of these first-order FRFs, denoted by $H(\omega, V_{in})$ are shown with respect to the excitation amplitude in Figure 4. In addition, the first-order displacement-voltage FRFs, denoted by $H_P(\omega, V_{in}) = -H(\omega, V_{in})/m_p\omega^2$, are illustrated for the purpose of identifying ω_{max}, where the nonlinear effects are greatest.

The plots in Figure 4 indicate that the peak resonance shifts upwards as the excitation amplitude increases, even when relatively low excitation amplitudes are used. It can be inferred from this information that the stiffness of the suspension rises with the proof-mass displacement $x(t)$, thereby increasing the excitation amplitude required for the proof-mass to reach the stroke length relative to the linear (constant stiffness) case. Additionally, Figure 4 shows that there is a smooth, continuous transition in the FRFs as the excitation amplitude increases, from the small degree of FRF distortion at low excitation amplitudes to the jump phenomenon that occurs at the higher excitation amplitudes. However, the presence of stroke saturation at $V_{in} = 0.4$ V is noticeable by the abrupt increase in the sharpness of the peak resonance.

It should be noted that the peak resonance frequency of $H(\omega, V_{in})$ in Figure 4 is significantly higher than the peak resonance frequency ω_{max} in Figure 5 when low excitation amplitudes are used, such that the maximum force amplitude does not correspond to the maximum displacement amplitude. Thus, the nonlinear effects observed in the force-time signals in Figure 2 are relatively independent of the amplitude of the force-signal time signal in question. An example of this can be seen in Figure 2 at $V_{in} = 0.3$ V; the amplitude levels of the two signals are similar, yet the lower-frequency signal contains far more harmonic distortion than its higher-frequency counterpart.

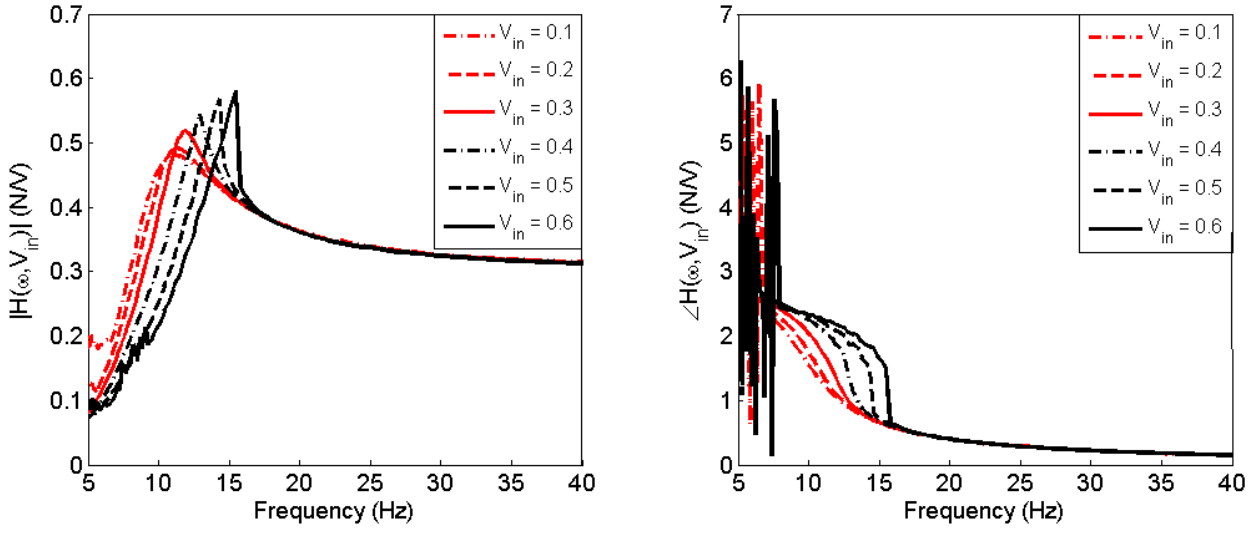

a) (b)

Figure 4: Actuator force-voltage FRFs, with (a) magnitude and (b) phase.

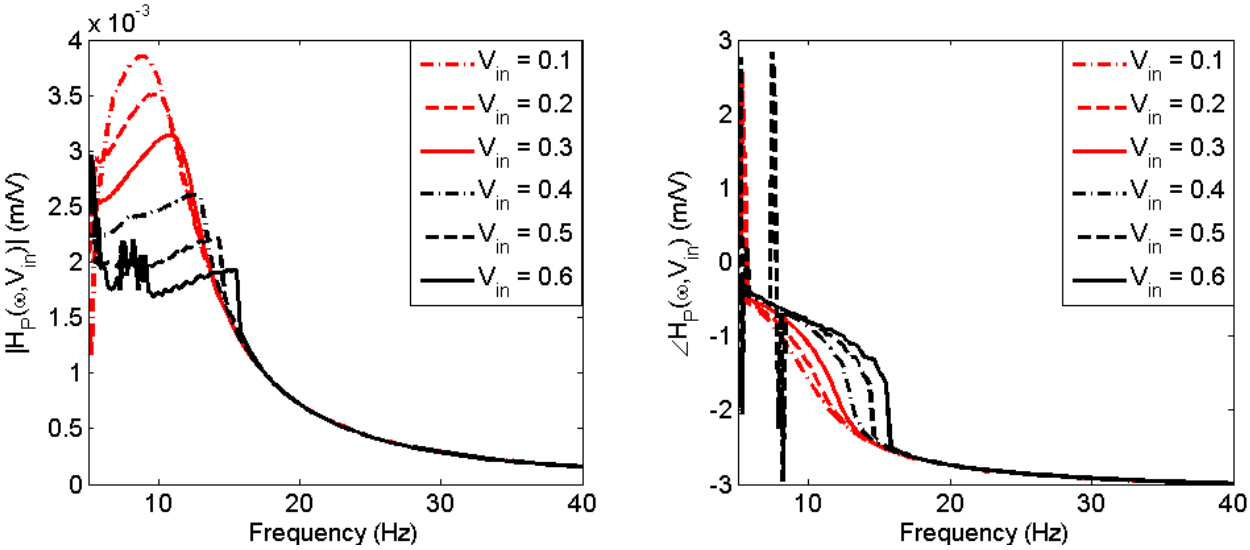

a) (b)

Figure 5: Actuator displacement-voltage FRFs, with (a) magnitude and (b) phase.

An examination of the displacement-force FRFs in Figure 5 reveals that the magnitude of the peak resonance decreases with increasing excitation amplitude, whilst the peak resonance frequency rises and exhibits the jump phenomenon at high excitation levels. These characteristics are commonly found in the first-order receptance FRFs of a hardening Duffing oscillator, which is typically used to model systems with low-order polynomial nonlinearities [6]. These observations further reinforce the notion that a nonlinear hardening stiffness is present in the suspension, regardless of the effects of stroke saturation.

4. SIMULATIONS

Since the primary focus of this study is to model the effects of stroke saturation, it appears reasonable to ignore the additional suspension nonlinearities discovered in the previous section, in order to simplify the model. The first step of this modelling procedure is to determine the equations of motion used for the linear piecewise model, defined in part by Nagurka and Huang [7]. It was shown in Figure 2 that stroke saturation is an asymmetrical phenomenon as a result of the proof-mass colliding with one particular end stop. For this reason, the proof-mass displacement was limited in the negative direction by the stroke length $\mathrm{d} = -1\,\mathrm{mm}$, with no bounds imposed in the positive direction. The resulting equations are:

$$\begin{cases} m_p\ddot{x}(t) + (c_p + c_s)\dot{x}(t) + (k_p + k_s)(x(t) - d) = f(t), \; x(t) < d \\ m_p\ddot{x}(t) + c_p\dot{x}(t) + k_p x(t) = f(t), \; x(t) \geq d \end{cases} \tag{2}$$

where $x(t)$ is the displacement of the proof-mass, m_p, c_p, k_p represent the linear suspension parameters, and c_s, k_s characterise the stiffness and damping parameters of the proof-mass/end stop impact. The restoring force provided by the linear suspension and the end stops is illustrated as a function of the proof-mass displacement in Figure 6 below.

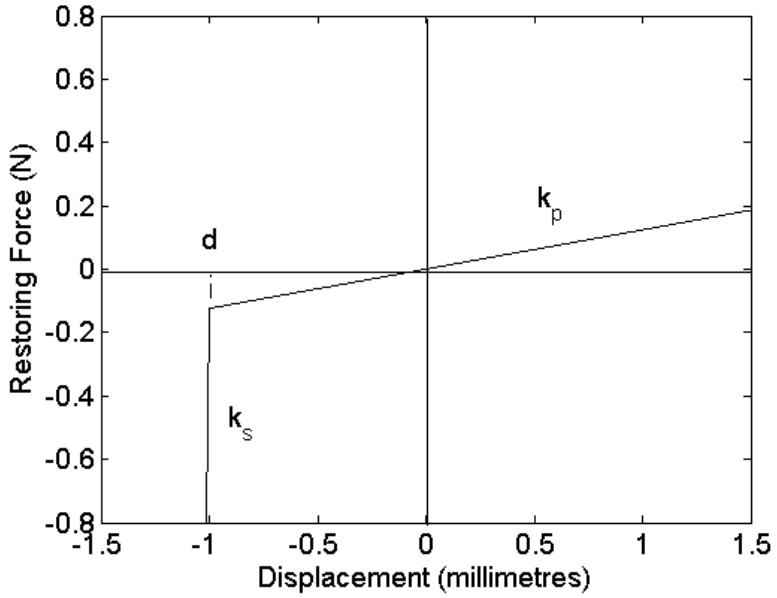

Figure 6: One-sided linear piecewise model of the actuator.

The next step is to obtain the model parameters from the experimental data given in the previous section. The linear suspension parameters are obtained by curve-fitting a model to the measured FRF with the lowest excitation amplitude, such that the actuator is operating in its linear regime. By applying Premount's derivation for the linear actuator FRF [10], the modelled force-voltage FRF $H_{mod}(\omega)$ at low levels of excitation can be written as:

$$H_{mod}(\omega) = \frac{-g\omega^2}{\omega_p^2 + j2\zeta_p\omega_p\omega - \omega^2} \tag{3}$$

Here, g is a gain term that is determined by the product of the amplifier gain, the magnetic flux of the actuator coil, and the electrical admittance of the actuator coil. Additionally, ω_p and ζ_p denote the natural frequency and apparent damping ratio of the actuator, taking into

account the counter-electromotive force. The curve-fitting procedure is first implemented [11] to obtain ω_p and ζ_p. Manufacturer data [9] states that $m_p = 0.032\,\text{kg}$, and so the stiffness and damping parameters k_p and c_p can be obtained from ω_p and ζ_p.

4.1 Impact Parameters

In order to establish k_s and c_s, it is necessary to consider the impact parameters, such as the contact time and the coefficient of restitution. Nagurka and Huang [7] demonstrated that the contact time ΔT of an impact can be established by modelling the impact as a half-sine of frequency ω_s, which is typically much higher than the excitation frequency. Using this definition, ω_s can be related to ΔT using:

$$\omega_s = \frac{\pi}{\Delta T} \approx \sqrt{\frac{k_s}{m_p}} \tag{4}$$

assuming that $k_s >> k_p$. Since the contact time can be observed experimentally, rearranging Eq. (4) results in an expression for k_s in terms of known parameters:

$$k_s = m_p\left(\frac{\pi}{\Delta T}\right)^2 \tag{5}$$

The relationship between k_s and ΔT is shown in Figure 7.

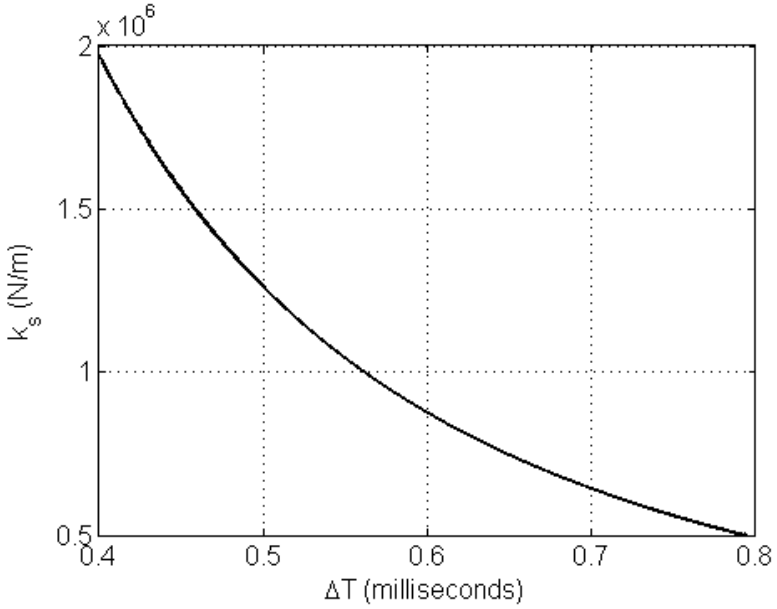

Figure 7: Variation of the end stop stiffness k_s and the contact time ΔT. It can be seen that k_s is very sensitive to small changes in ΔT when the contact time is small.

The average contact time can be found from the duration of the spikes in the measured force-time histories, and are shown in Figure 8(a) below as a function of excitation amplitude and frequency. Furthermore, the relative unbiased standard deviation, denoted by RSD, is shown in Figure 8(b) for the purpose of examining the consistency of the spikes, where:

$$RSD = \frac{\sum_{n=1}^{N}\left(\Delta T_n - E[\Delta T]\right)^2}{E[\Delta T](N-1)} \tag{6}$$

N being the number of spikes in the force-time history in question.

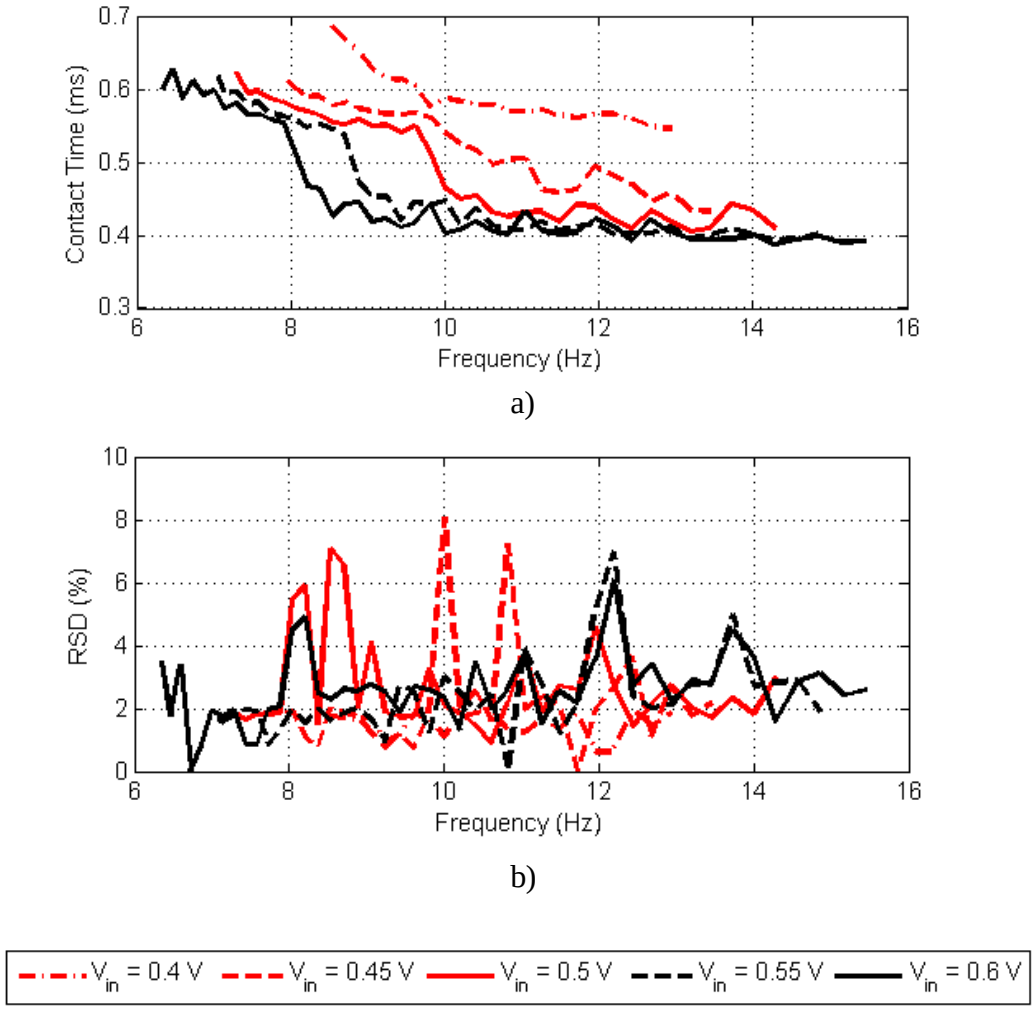

Figure 8: Spike properties in the force-time histories, where (a) is the average contact time in milliseconds and (b) is the relative standard deviation.

It is apparent that the average contact time varies significantly with excitation amplitude and frequency, ranging from 0.4 milliseconds at high excitation amplitudes and frequencies to 0.7 milliseconds at the other end of the scale. Since k_s is inversely proportional to ΔT^2, it is very sensitive to small changes in the contact time, and so the range of possible values is considerable. This indicates that the total actuator stiffness continues to increase after stroke saturation has started to occur. Despite the large uncertainty ($\pm 60\%$), a single value for k_s is chosen by averaging over frequency and amplitude. However, the small RSD values in Figure 8(b) indicate that the contact times are remarkably consistent over the force-time histories.

Since there is no easy way of establishing the coefficient of restitution from the force-time signals, it is assumed that the coefficient of restitution is approximately unity, which yields a negligible value for c_s [7]. The values of each of the model parameters are shown in Table 2.

Parameter	m_p	c_p	k_p	c_s	k_s	g
Value	0.032 kg	1.3 Ns/m	124 N/m	0 Ns/m	1.3×10^6 N/m	0.3 N/V

Table 2: Measured actuator parameters.

These parameters were used to construct the linear piecewise actuator model in Simulink, where the force-time histories were simulated over a period of ten seconds using the ode3 solver, with a sample rate of 51.2 kHz. These simulated signals can be compared to the measured signals after undergoing similar processing.

5. COMPARISONS

First, a time-domain comparison is conducted, based on the results in Figure 2. Here, the measured signals are compared with the equivalent simulated signals, as shown in Figure 9.

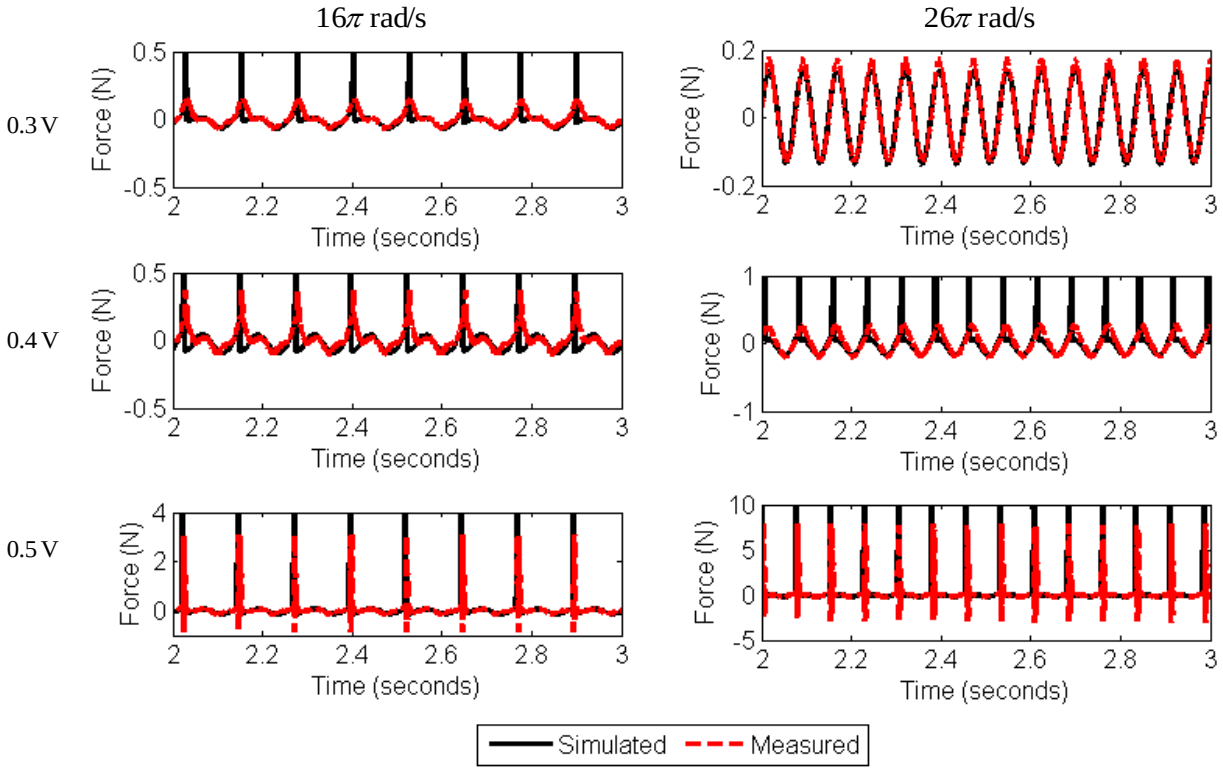

Figure 9: Comparison of simulated (black) and measured (red) signals.

In Figure 9, it is apparent that the spikes present in the measured signals when stroke saturation occurs also appear in the simulated signals, thereby indicating that stroke saturation can be fundamentally modelled as a rapid change in stiffness. However, there are a number of discrepancies. Firstly, in a few cases, the simulated force-time signals incorrectly indicate that stroke saturation is occurring e.g. $\omega = 16\pi$ rad/s, $V_{in} = 0.3$ V. Secondly, the simulated signals for $\omega = 16\pi$ rad/s do not feature the low-order harmonic distortion present in the measured signals. Thirdly, the spikes in the simulated signals are greater in magnitude that in the measured signals. It is believed that the first two issues can be overcome through the introduction of a simple nonlinear polynomial stiffness term in Eq. (2), since the nonlinearity will increase the excitation amplitude required for stroke saturation, and will introduce the necessary harmonics. The third issue can be attributed to the constant value chosen for k_s since this parameter controls the magnitude and duration of the spikes.

In short, more accurate time-domain simulations could be obtained by continuously varying the stiffness, as is used in the model derived by Baumann and Elliott [4]. However, the agreement between simulation and measurement is good when both signals are approximately sinusoidal, as is the case for $\omega = 26\pi$ rad/s, $V_{in} = 0.3$ V.

Finally, a frequency-domain comparison is undertaken on the first-order simulated and measured FRFs, based on the results in Figure 4. The magnitudes are compared using $V_{in} = 0.1$ V to 0.6 V in Figure 10.

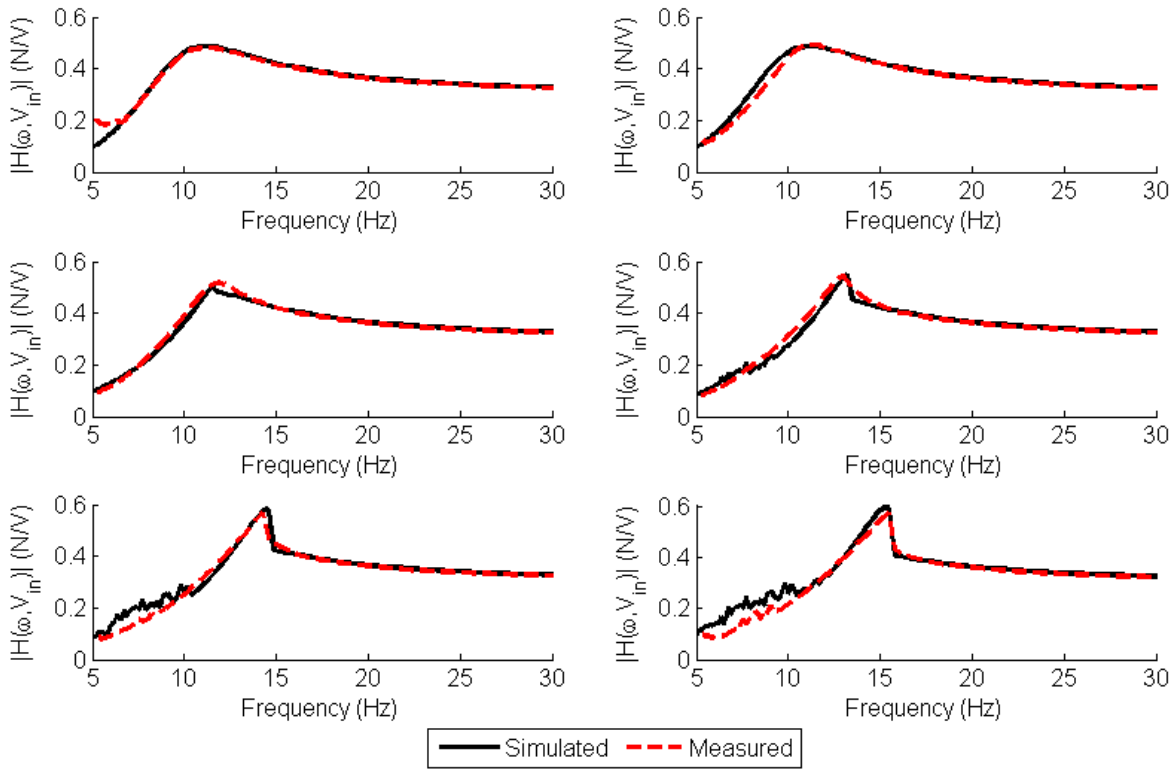

Figure 10: Comparisons of simulated (black) and measured (red) first-order FRFs, where (a) $V_{in} = 0.1\,V$ (b) $V_{in} = 0.2\,V$ (c) $V_{in} = 0.3\,V$ (d) $V_{in} = 0.4\,V$ (e) $V_{in} = 0.5\,V$ (f) $V_{in} = 0.6\,V$.

In Figure 10, the best agreement between the simulated and measured FRFs happens when the actuator behaves in an approximately linear manner (Figure 10(a)) or when the jump phenomenon occurs (Figures 10(e) and 10(f)). Whilst agreement is also good at intermediate excitation amplitudes, small discrepancies occur between the simulated and measured FRFs, with two noticeable differences. Firstly, the piecewise model is linear beneath the saturation threshold, and so the simulated FRF does not initially vary with amplitude, as can be seen from the discrepancy in Figure 10(b). Secondly, the simulated FRFs change very rapidly from being entirely linear to the jump phenomenon being observed, as is apparent in Figure 10(c) and 10(d). In contrast, the measured FRFs vary continuously between these two extremes.

To summarise, the simulated FRFs can be used to predict the measured FRFs with a reasonable degree of accuracy, particularly concerning the peak resonance. However, it is entirely possible to have apparently accurate results in the frequency-domain when considerably less agreement is observed in the time-domain signals, as is shown in Figure 9. This occurs because the first-order FRFs only reveal information about the steady-state amplitude at the fundamental frequency. Therefore, the discrepancies can be explained by the higher-order FRFs of the inertial actuator, which represent the actuator response at harmonics of the fundamental forcing frequency.

6. CONCLUSIONS AND FUTURE WORK

A linear piecewise model of an inertial actuator undergoing stroke saturation was derived for the purpose of assessing closed-loop performance and stability when using proof-mass actuators for active vibration control. The model parameters were estimated from experimental measurements of the actuator, where the force-time histories of the actuator were recorded for a variety of excitation amplitudes and frequencies. In addition, the experimental measurements were used to analyse the actuator dynamics in the time- and frequency-domains.

It was found that harmonic distortion was present in the time-histories when the excitation frequency was close to the peak resonance of the proof-mass displacement, even when the excitation amplitude was below the saturation threshold. This phenomenon was attributed to weak hardening nonlinearities in the proof-mass suspension. It was also noted that the stiffness of the end stop appeared to increase with excitation amplitude once stroke saturation started to occur, as a result of reductions in the contact time. Although there was good agreement between the model simulations and the measurements in the frequency-domain, obvious discrepancies were present the time-domain, as the changes in stiffness had not been included.

Although the linear piecewise model is a reasonable starting point for emulating stroke saturation, a more accurate model could be derived by considering the continuously changing stiffness, as used by Baumann and Elliott [4], with the inclusion of a low-order polynomial stiffness term. An investigation into this type of model will form the basis of future work.

ACKNOWLEDGEMENTS

Laurence Wilmshurst's Ph.D is supported by a Rayleigh scholarship from the University of Southampton.

REFERENCES

[1] D. J. Wagg, S. A. Neild. *Nonlinear Vibration with Control – For Flexible and Adaptive Structures* (*Solid Mechanics and Its Applications)*. Springer. 2009.

[2] D. K. Lindner, G. A. Zvonar, D. Borojevic. Performance and Control of Proof-Mass Actuators Accounting For Stroke Saturation. *AIAA Journal of Guidance, Dynamics and Control*, 17(5). 1103-1108, 1994.

[3] J. G. Chase. M. Yim, A. A. Berlin. Integrated centering control of inertially actuated systems. *Control Engineering Practice*, 7, 1079-1084, 1999.

[4] O. N. Baumann and S. J. Elliott. Destabilization of velocity feedback controllers with stroke limited inertial actuators. *Journal of the Acoustical Society of America*, 121(5), 2007.

[5] J. G. Chase, H. A. Smith, Robust H_∞ control considering actuator saturation. I: Theory, *Journal of Engineering Mechanics*, 122, 976-983, 1996.

[6] K. Worden and G.R. Thomlinson. *Nonlinearity in structural dynamics: Detection, identification, and modelling.* CRC Press. 2001.

[7] M. Nagurka, S. Huang. A Mass-Spring-Damper Model of a Bouncing Ball. *International Journal of Engineering Education.* 22(2), 393-401, 2006.

[8] D. M. Storer, G. R. Tomlinson. Recent Developments in the Measurement and Interpretation of Higher Order Transfer Functions from Non-Linear Structures. *Mechanical Systems and Signal Processing*, 7(2), 173-189, 1991.

[9] Micromega Dynamics, Active Damping Devices and Inertial Actuators, http://www.micromega-dynamics.com/doc/ADD_Catalog_Rev2.pdf

[10] A. Preumont, *Vibration control of active structures: an introduction.* 2nd ed. Springer, 2002.

[11] D. Formenti and M. Richardson, Parameter estimation from frequency response measurements using rational fraction polynomials. *Proceedings of the First International Modal Analysis Conference*, Orlando, FL, 1982.